AIP | Review of Scientific Instruments

Free-flight measurement technique in the free-piston high-enthalpy shock tunnel

H. Tanno, T. Komuro, K. Sato, K. Fujita, and S. J. Laurence

Citation: Review of Scientific Instruments **85**, 045112 (2014); doi: 10.1063/1.4870920
View online: http://dx.doi.org/10.1063/1.4870920
View Table of Contents: http://scitation.aip.org/content/aip/journal/rsi/85/4?ver=pdfcov
Published by the AIP Publishing

Free-flight measurement technique in the free-piston high-enthalpy shock tunnel

H. Tanno,[1,a)] T. Komuro,[1] K. Sato,[1] K. Fujita,[2] and S. J. Laurence[3,b)]
[1]*Japan Aerospace Exploration Agency, Kakuda Space Center, Kakuda Miyagi 981-1525, Japan*
[2]*Japan Aerospace Exploration Agency, Chofu Aerospace Center, Chofu Tokyo 182-8522, Japan*
[3]*German Aerospace Center, Institute of Aerodynamics and Flow Technology Spacecraft Department, Bunsenstr.10, 37073 Göttingen, Germany*

(Received 4 January 2014; accepted 30 March 2014; published online 15 April 2014)

A novel multi-component force-measurement technique has been developed and implemented at the impulse facility JAXA-HIEST, in which the test model is completely unrestrained during the test and thus experiences free-flight conditions for a period on the order of milliseconds. Advantages over conventional free-flight techniques include the complete absence of aerodynamic interference from a model support system and less variation in model position and attitude during the test itself. A miniature on-board data recorder, which was a key technology for this technique, was also developed in order to acquire and store the measured data. The technique was demonstrated in a HIEST wind-tunnel test campaign in which three-component aerodynamic force measurement was performed on a blunted cone of length 316 mm, total mass 19.75 kg, and moment of inertia 0.152 kgm^2. During the test campaign, axial force, normal forces, and pitching moment coefficients were obtained at angles of attack from 14° to 32° under two conditions: $H_0 = 4$ MJ/kg, $P_0 = 14$ MPa; and $H_0 = 16$ MJ/kg, $P_0 = 16$ MPa. For the first, low-enthalpy condition, the test flow was considered a perfect gas; measurements were thus directly compared with those obtained in a conventional blow-down wind tunnel (JAXA-HWT2) to evaluate the accuracy of the technique. The second test condition was a high-enthalpy condition in which 85% of the oxygen molecules were expected to be dissociated; high-temperature real-gas effects were therefore evaluated by comparison with results obtained in perfect-gas conditions. The precision of the present measurements was evaluated through an uncertainty analysis, which showed the aerodynamic coefficients in the HIEST low enthalpy test agreeing well with those of JAXA-HWT2. The pitching-moment coefficient, however, showed significant differences between low- and high-enthalpy tests. These differences are thought to result from high-temperature real-gas effects. © *2014 AIP Publishing LLC*. [http://dx.doi.org/10.1063/1.4870920]

I. INTRODUCTION

In the first flight of the Space Shuttle, unexpected pitch-up was found during the hypersonic gliding phase. The body-flap deflection angle for pitch trim had to be twice that predicted in preflight wind-tunnel tests.[1] The post-flight analysis implied that one of the major causes of this deflection-angle discrepancy was high-temperature real-gas effects.[2,3] In high-temperature flows, oxygen and nitrogen molecules can be partially or fully dissociated; as a result, the pressure on the nose of a reentry vehicle becomes slightly higher than in a perfect-gas flow, while the pressure on the aft of the vehicle decreases slightly. Integrating the surface pressure results in a shifting forward of the c.p. (center of pressure), so that the total pitch moment produces a higher nose-up attitude than under perfect-gas conditions. The high-enthalpy shock tunnel HIEST[4] (Fig. 1) was originally built to study such high-temperature real-gas effects on reentry vehicle aerodynamics. This tunnel can be operated at stagnation pressures up to 150 MPa and stagnation enthalpies up to 25 MJ/kg, under which conditions test times of 2 ms or longer are attainable. Nevertheless, the measurement of aerodynamic forces in HIEST presents significant technical difficulties due to the short test duration and high free-stream dynamic pressure compared with conventional wind tunnels. When a conventional force-balance measurement technique was used in HIEST,[5] one of the major technical issues encountered was mechanical vibration, principally from the sting, which became progressively worse with increasing free-stream dynamic pressure. These vibrations, composed of several frequency modes, were not damped out within the milliseconds of the test duration, resulting in large-scale oscillations in the measured signals. This problem usually degrades the time response to the extent that the measurement precision is insufficient to detect real-gas effects. To address this issue, a force-measurement technique called the accelerometer balance technique[6] was applied in HIEST, using weakly restrained test models with on-board miniature accelerometers.[7] The model is suspended by two thin wires, leaving it free to move; aerodynamic forces are thus simply obtained as products of the measured accelerations and the mass of the model. Although this technique mitigated the vibrations from the support system and allowed substantially improved force-measurement precision, the suspension wires were subject to a significant parasitic drag force, which became another source of uncertainty.

a)Electronic mail: tanno@spaceships.isas.jaxa.jp
b)Present address: Department of Aerospace Engineering, University of Maryland, College Park, Maryland, 20742, USA.

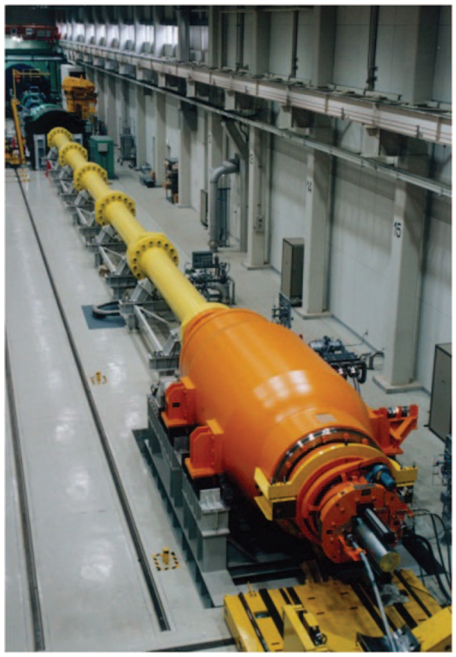

FIG. 1. Free-piston shock tunnel HIEST.

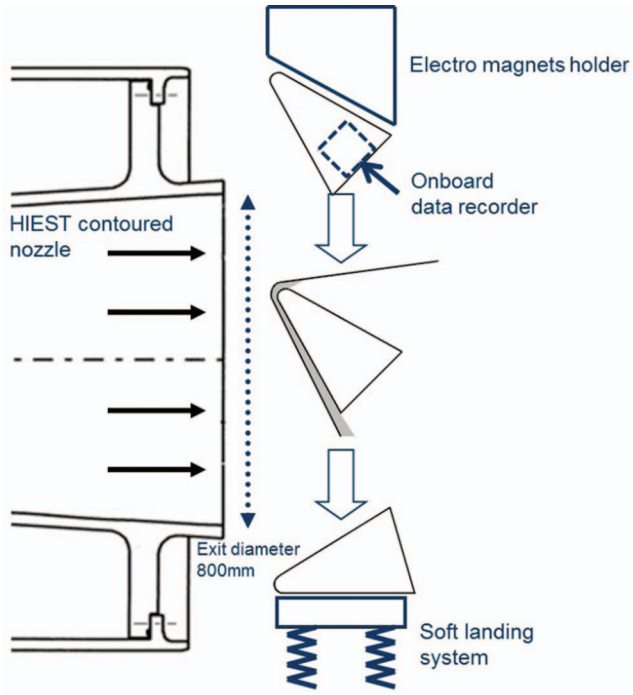

FIG. 2. The "Free-flight force measurement technique."

To resolve these concerns, a new free-flight force-measurement technique with completely unrestrained test models was developed. Such techniques have been implemented by previous researchers; a good summary can be found in Naumann *et al.*[8] Most previous work was based on optical measurements using a high-speed camera system.[9] Displacements were obtained directly from test-model images, and accelerations were then derived by double differentiation of the displacement curves. However, this differentiation produces significant amplification of the measurement noise; moreover, since the accuracy of the measurement depends on the model displacement, lightweight models are generally favored. This, though, can lead to variations in the model position and angle of attack during the test. In order to improve the measurement accuracy, Naumann *et al.*[8] used direct acceleration measurements with miniature accelerometers mounted inside the model in experiments carried out in a shock tunnel. Through a cleverly designed model injection and catching system, the test model could experience free-flight conditions over a duration of 10 ms. Nevertheless, the model injection system and umbilical at the aft of the model may have produced aerodynamic interference with the model wake flow; such interference would become especially undesirable when pitching-moment measurements are required at high angles of attack.

In the present technique, the model is released from a magnetic holder installed on the wind-tunnel ceiling so that it arrives in the nozzle core in synchrony with the arrival of the test flow. During the entire test duration, the model is thus completely unrestrained by any support system and therefore free both aerodynamically and mechanically. Since a comparatively heavy model can be used with this technique, variation of model position and attitude can be made negligible during the test period, even in the high dynamic-pressure conditions of HIEST. Moreover, acceleration measurement accuracy can be ensured with on-board accelerometers whose outputs are stored in an on-board miniature data recorder. After the conclusion of the test flow, the model falls into a soft-landing system placed on the floor, enabling the model and instruments to be reused. This sequence of events is shown in Fig. 2.

The present article describes the implementation of this "free-flight force measurement technique" in the HIEST shock tunnel. First, we provide details of the apparatus developed for this technique: a miniature on-board data recorder, the test model and the model releaser/catcher. The accuracy and precision of three-component aerodynamic force measurements are then discussed with reference to experiments on a blunted cone. Comparison between low- and high-enthalpy test conditions (i.e., perfect-gas and real-gas conditions) verify the previously documented real-gas effect on aerodynamics noted earlier, namely, an increased nose-up tendency in the pitch.

II. FREE-FLIGHT MEASUREMENT

A. Miniature data recorder

For the present "free-flight" aerodynamic measurements, an on-board miniature data recorder is the most important technology. In determining aerodynamic forces and moments with acceleration measurements, since two accelerometers are required for the force and moment on each axis, at least six accelerometers are necessary for six-component measurements. Moreover, recording of the free-stream Pitot pressure is also essential to be able to normalize the forces and obtain aerodynamic coefficients. The recorder should thus be designed to accommodate six channels for piezoelectric sensors (PCB Piezotronics Inc. ICP type sensors) for accelerometers and a few channels for piezoresistive sensors (Kulite

TABLE I. Specifications of the miniature data recorder.

Sensor type	Piezoelectric ICP type (PCB) and piezoresistive (Kulite)
Number of channels	10 (six channels for piezoelectric and four channels for piezoresistive)
Input	−10 V to 10 V
Resolution	16 bit
Sampling rate	500 kHz (for each channel)
Duration	400 ms
Pre-trigger	Adjustable from −400 to 0 ms with on-board micro switch
Trigger arm system	IR photo-switch (with LED indicator)
Size	50 mm × 70 mm × 40 mm
Battery life	2 h
Interface	USB

Semiconductor Products, Inc.) for pressure measurement. Since the test time in HIEST is on the order of milliseconds, a high sampling rate of 500 kHz is crucial and 16-bit measurement accuracy is essential. In addition, the recorder must include batteries with sufficient storage to ensure a run time of 2 h, but which must also be small enough to mount within the limited space inside the model. The required specifications for the data recorder as just described are summarized in Table I.

Unfortunately, there is no commercially available data recorder that satisfies these requirements; a special-purpose data recorder was therefore designed and manufactured at JAXA.[10] As shown in the circuit diagram of the recorder (Fig. 3), a custom-made LSI reads the measured signals from the A/D converter and stores digitized data in the static memory. The recorder was designed to maximize operating speed and to minimize size: a four-layer circuit board was adopted, which resulted in recorder dimensions of 100 mm (L) × 100 mm (W) × 70 mm (H).

The total measurement capacity of the recorder is 800 ms, which is determined by the size of the on-board memory. The recorder has a pre-trigger system that can be adjusted arbitrarily with micro-switches. In order to arm the trigger, the recorder also has an IR photo switch and a LED indicator that shows the status of the recorder. After each wind-tunnel test, data stored in the static memory of the recorder were transferred to a host PC through a USB interface (Fig. 4).

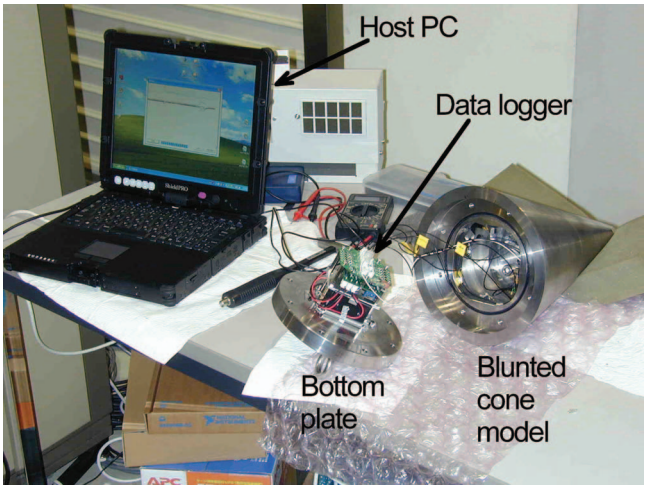

FIG. 4. Miniature data recorder with a blunt cone after a shot. For data transfer, the recorder was connected to the host PC via USB interface.

B. Wind tunnel test model

The test model, as shown in Fig. 5, was a 316 mm long blunted cone with a half-angle of 15°, a nose-tip radius of 20 mm and a base diameter of 200 mm. As will be described shortly, high-power electromagnets on the ceiling of the HIEST test section were used to hold and release the model. Due to concerns that the intense field produced by the electromagnets might interfere with the electrical components of the data recorder inside the model, the cone was manufactured from a ferromagnetic material, stainless steel SUS410, in order to function as a shield to prevent the electromagnetic field from penetrating inside the model.

The total mass of the cone was 19.75 kg, including the internal instrumentation which consisted of the data recorder with batteries, six piezoelectric accelerometers (PCB Piezotronics Inc. type-352C65) and one piezoresistive pressure transducer (Kulite semiconductor products Inc. type-XCQ093). Theoretically, this would allow six-component

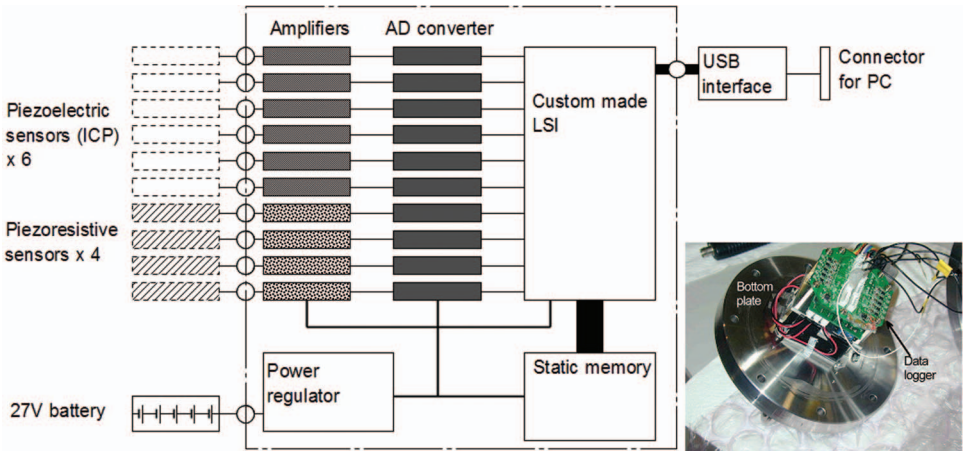

FIG. 3. Block diagram of the on-board data recorder.

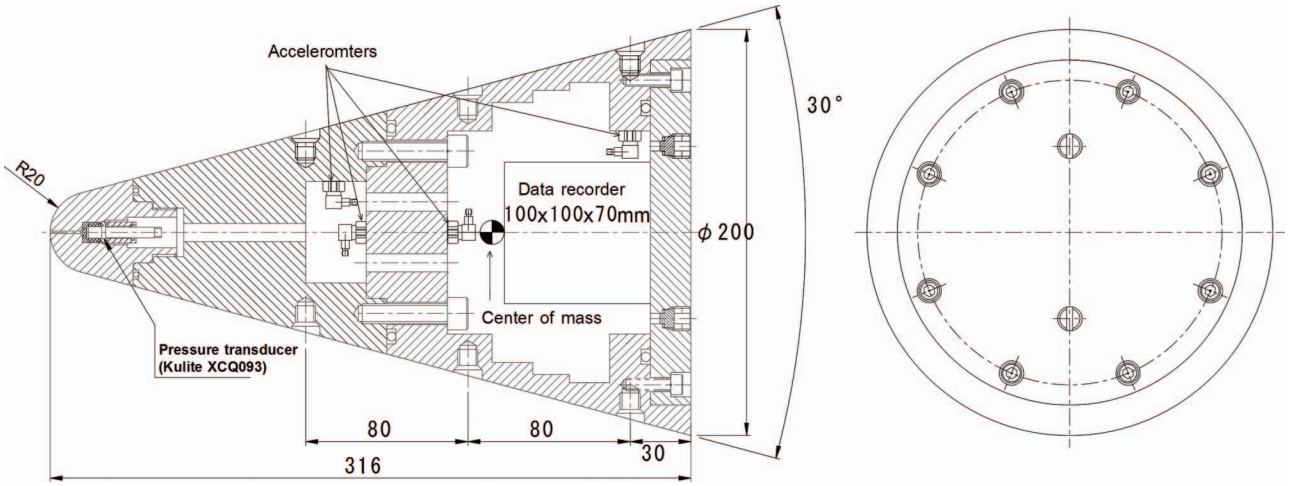

FIG. 5. Schematic of the blunted cone used in this study. The location of the center of mass was 156 mm from the nose tip. The model has an internal cavity in which the miniature data recorder can be installed. Six accelerometers for axial force, nominal force, and pitching moment were instrumented inside the model; four of the six accelerometers are shown in the figure.

force measurement; in this test campaign, however, only three components were measured: the axial force F_A, normal force F_N, and pitching moment M_y. Two accelerometers were configured to measure each of these aerodynamic components. The pressure transducer was mounted in the tip of the model nose to obtain the free-stream Pitot pressure as the basis for calculating aerodynamic coefficients. Although the recorder has 4 channels for piezoresistive pressure transducers, the remaining channels were blanked in this campaign. For such three-component measurements, the moment of inertia about the center of mass must be known to determine the pitching moment. A generic two-wire pendulum method was used to measure the moment of inertia; the obtained value was 0.152 kgm^2. The location of the center of mass was also measured with the technique, giving a position 156 mm from the nose tip.

Prior to each test, the HIEST test section was evacuated to ~2 Pa, which was then held for approximately 1 h. When designing the cone, we aimed to retain atmospheric pressure inside the model, because the electrical devices, in particular the batteries and capacitors in the recorder, were not certain to function in a vacuum. The cavity containing the recorder was therefore designed to act as a pressure chamber and was sealed with O-rings. It was verified to be airtight at the required pressure level for at least 2 h.

C. Model releaser and catcher

As shown in the photographs of the model set-up in the HIEST test section (Fig. 6), the model is initially suspended by two electromagnets, which were capable of holding 60 kg. Since the test model must lie in the nozzle core flow simultaneously with the test flow arrival, the release system must respond rapidly to the trigger signal from tunnel initiation with millisecond-order accuracy. The release system was able to vary the model angle of attack from 0° to 40°. The prototype of the releaser developed in the study was located 400 mm above the axis of the nozzle center to avoid damage to the magnets from the high-temperature hypersonic test flow, as well as from the high-speed particles often produced as main-diaphragm debris. Thus, upon test flow arrival, the model must have fallen the 400 mm from the releaser to the nozzle center. Since 400 mm of free-fall requires approximately 280 ms, the trigger signal to drop the model must arrive 280 ms before the test flow does. In the present test campaign, the trigger signal was picked up from the piston launch system of the facility, which is the most up-stream section of HIEST; this signal was registered 400 ms before the flow arrival in the

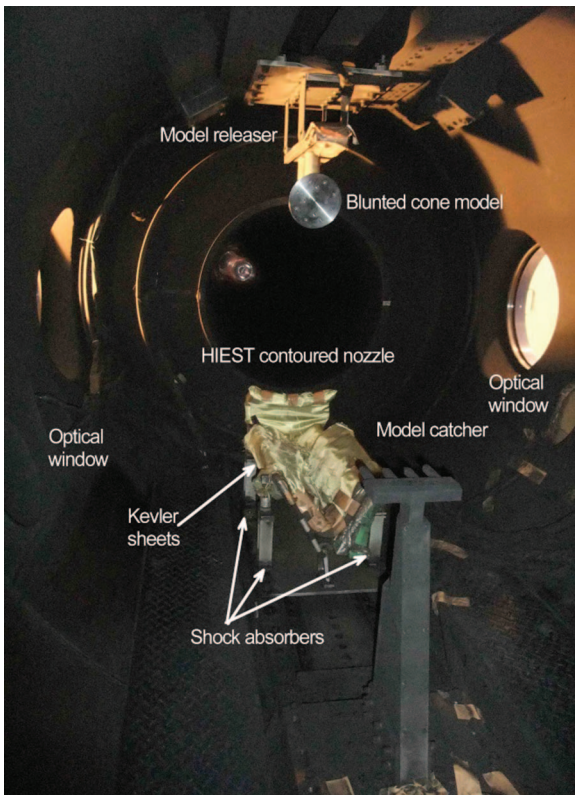

FIG. 6. Model releaser and model catcher in the HIEST test section. The blunted cone model is held by the two electromagnets to the ceiling of the HIEST test section with an angle of attack of 17°.

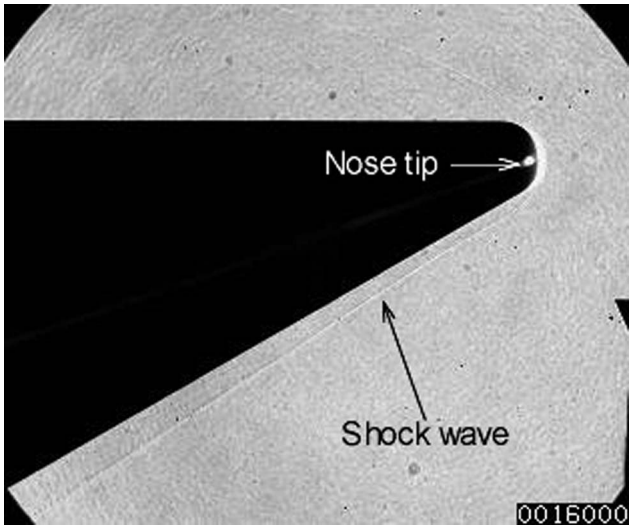

FIG. 7. Example of a Schlieren image used to monitor the model motion (condition 1; flow is right to left).

test section. To adjust the timing of the model release, a digital controller was developed to deactivate the electromagnets at a precise time. The controller included a sequencer, electrical relays, and the digital delay.

Following the conclusion of the test, the cone falls onto the catcher located on the bottom of the HIEST test section, having reached a final speed of less than 10 m/s. In order to avoid damage to the model and allow its reuse, the intensity of this impact had to be mitigated. The catcher thus had four hydraulic dampers to absorb impact energy, and shock-absorbing polymer sheets were also placed on the catching surface of the system. Furthermore, the data recorder was installed in the model with an anti-shock mounting. These steps minimized the impact deceleration of the model and data recorder, allowing reuse of the complete system over the entire measurement campaign.

D. Model movement during free flight

As already mentioned, one of the critical issues encountered in free-flight measurement techniques is the variation in position and attitude of the model during the test duration. Here, an optical monitoring technique[11,12] was adopted to observe the model motion, with sequential Schlieren images recorded by a high-speed video camera (SHIMADZU Corp. Hypervision). An example of a Schlieren image is shown in Fig. 7 and typical displacement profiles in the x and y directions, as well as the pitch angle history, are presented in Fig. 8. Throughout the present test campaign, the 2σ-variation of the cone location and the angle of attack at the time of the test-flow arrival were, respectively, maintained at less than ± 6 mm from the nozzle center and less than $\pm 0.2^\circ$ from the initial angle of attack.

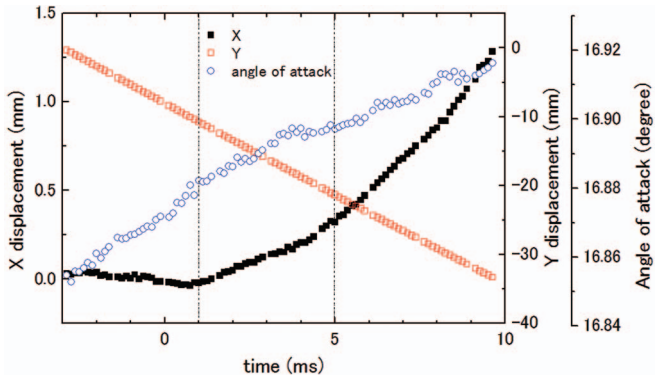

FIG. 8. X, Y displacements and angle of attack of the model recorded during a typical experiment. The dashed vertical lines indicate the approximate steady-state test time.

During the steady-state test time, the translational motion is seen to be approximately 0.3 mm in the x direction and 11 mm in the y direction; the change in angle of attack is less than 0.02°. We can thus be confident that any aerodynamic effects caused by changes in the model position or attitude during the test time are negligible.

III. HIEST WIND TUNNEL TEST RESULTS

A. Test flow conditions

The HIEST facility has two nozzles, one conical and one contoured. In this test campaign we used the contoured nozzle, which has an exit diameter of 800 mm, a nozzle throat of 50 mm, and an area expansion ratio of 256. Table II shows the test flow conditions selected in the campaign, which conditions were calculated with an axis-symmetrical in-house nozzle flow code.[13] Condition 1 was a low-enthalpy

TABLE II. Test flow conditions of HIEST and HWT2.

		HIEST condition 1	HIEST condition 2	HWT2
Stagnation (nozzle reservoir) condition	Pressure (MPa)	1.3×10^1	1.5×10^1	6.1
	Temperature (K)	3.0×10^3	7.6×10^3	1.1×10^3
	Enthalpy (MJ/kg)	3.8	1.6×10^1	N.A.
Free-stream condition	Temperature (K)	2.9×10^2	1.3×10^3	5.5×10^1
	Pressure (kPa)	1.1	2.1	1.7×10^{-1}
	Density (kg/m^3)	1.4×10^{-2}	4.8×10^{-3}	1.1×10^{-2}
	Velocity (km)	2.6×10^3	4.9×10^3	1.5×10^3
	Mach number	7.6	6.2	9.7
	Unit Reynolds number (/m)	2.0×10^6	4.5×10^5	8.7×10^5

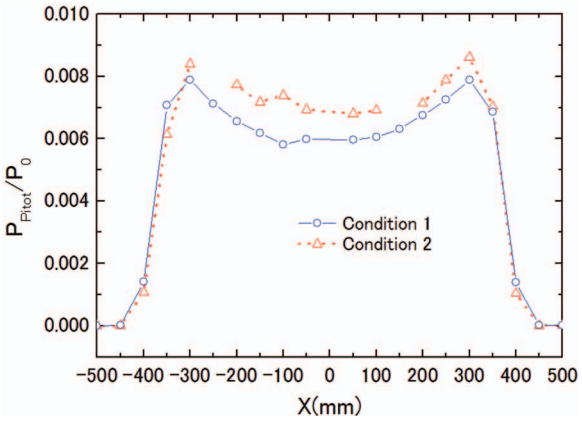

FIG. 9. Normalized Pitot pressure profiles obtained in the contoured nozzle calibration shots. Open circles and open triangles, respectively, indicate the results obtained under condition 1 (low-enthalpy) and condition 2 (high-enthalpy).

condition in which the flow could be approximated as a perfect gas, enabling measurements to be compared directly with results from the conventional blow-down wind tunnel JAXA-HWT2[14] to evaluate the accuracy of the technique. Condition 2 was a high-enthalpy condition with 85% dissociation of the oxygen molecules in the reservoir; high-temperature real-gas effects could thus be evaluated by comparison with the perfect-gas (i.e., condition 1) results.

In previous nozzle-calibration tests, Pitot pressure distributions under the two employed conditions were measured as shown in Fig. 9. The calibration test indicated that Pitot pressure deviation from the average value was ±3.1% within a 150 mm radius from the nozzle centerline circle in condition 1; for condition 2 this value was ±3.5% Based on this free-stream uniformity, the core of the test flow was defined as a 300 mm diameter circle in this test campaign.

B. Force measurement histories

Fig. 10 shows sequential high-speed video images of the falling cone taken with a monitoring video camera (CASIO EX-1). The timing of the release of the cone by the electromagnets was such that the cone was positioned in the core flow during the test period. After the conclusion of the shot, the cone was successfully soft-landed in the catcher. Throughout the test campaign, the cone and the instrumentation experienced no damage related to mechanical shocks. Fig. 11 shows examples of the time-resolved axial force coefficient, C_A, normal force coefficient, C_N, and pitching moment coefficient, C_M, under condition 1 at an angle of attack of 16.7°. All coefficients were obtained from the measured forces and moment by dividing by the product of the dynamic pressure q, and by the cross-sectional area of the cone. To obtain pitching moment, the model base diameter (D = 200 mm) was used as the reference length. Stagnation enthalpy affects the specific heat of the test flow, meaning that the relationship between the dynamic pressure and the Pitot pressure, Pt, varies slightly as q = 1.064pt and q = 1.07pt when H_0 is approximately 4 MJ/kg and 16 MJ/kg, respectively.

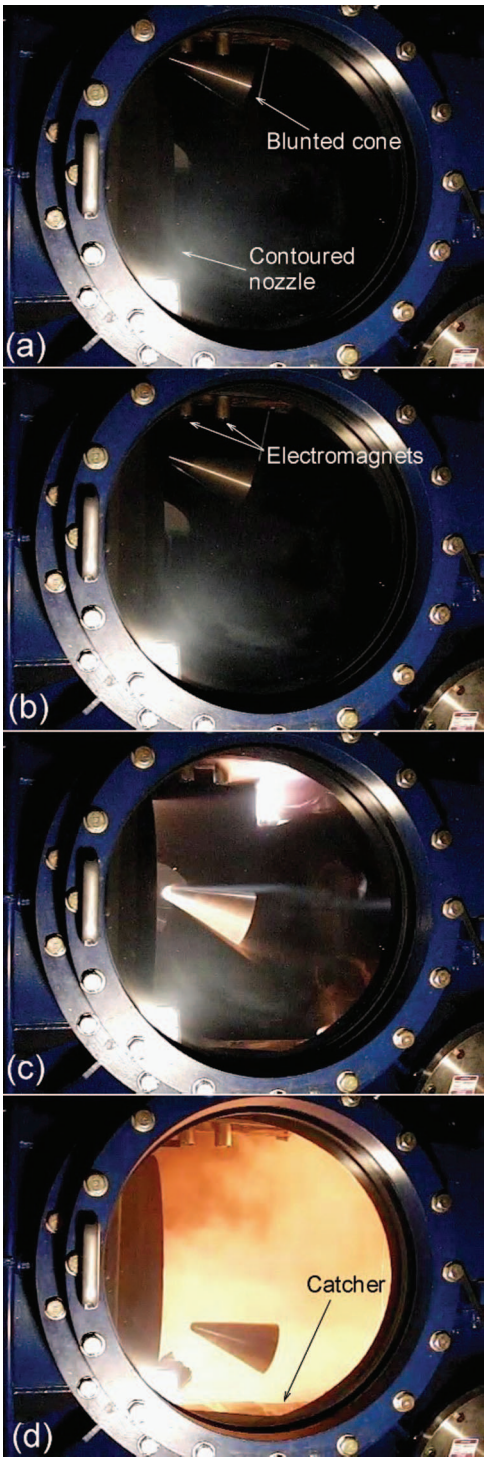

FIG. 10. Sequential images of the model dropping in the HIEST test section. (a) Model is suspended by the magnets. (b) Model has been released and is falling. (c) Test flow (from left to right) established around the model. (d) Test concluded; the model falls to the catcher.

IV. MEASUREMENT UNCERTAINTY

In Fig. 12, all the present measurements in HIEST, depicted as open symbols, show the relationship between aerodynamic coefficients and the angle of attack as the latter is varied from 14° to 32°, the coefficients being the average values during each shot. Circles and triangles in the figure show the results at condition 1 (perfect-gas condition) and

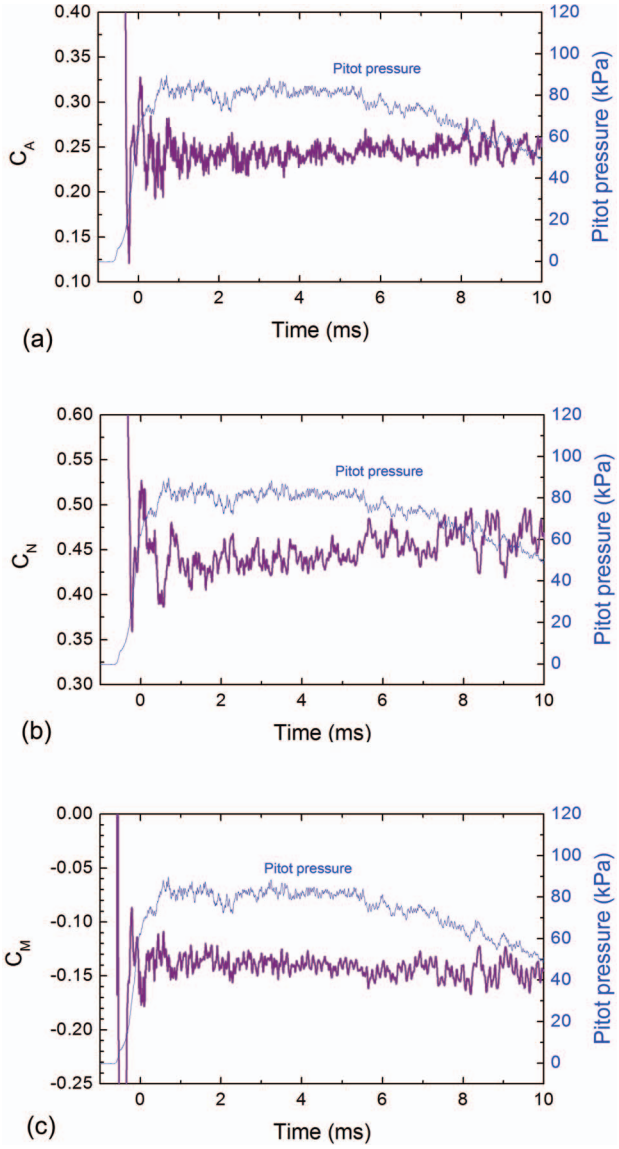

FIG. 11. Time records of aerodynamic coefficients obtained in shot #1908 (condition 1): Axial force coefficient C_A (a), normal force coefficient C_N (b), and pitching moment coefficient C_M (c) are shown as solid lines. The free-stream Pitot pressure history is also shown on each plot as a thin line.

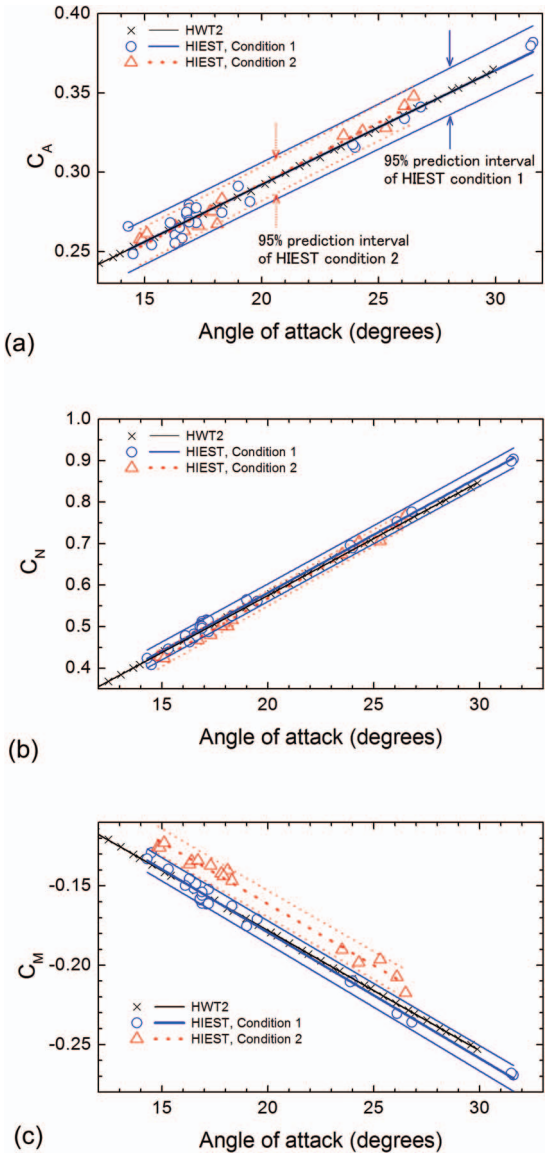

FIG. 12. Aerodynamic coefficients C_A(a), C_N(b), and C_M(c) for angles of attack from 14° to 32°. Open circles (condition 1) and triangles (condition 2) show the present measurements with the crosses indicating the results from the blow-down wind tunnel JAXA-HWT2 for comparison. 95%-PI (prediction intervals) defining the uncertainty limits for HIEST condition 1 and condition 2 are also shown, as thin lines.

condition 2 (real-gas condition), respectively. Aerodynamic coefficients measured in the blow-down hypersonic wind tunnel JAXA-HWT2 are also plotted as crosses and are used as a baseline under perfect-gas conditions to estimate the accuracy of the HIEST measurements. For the test campaign in HWT2, aerodynamic measurements with a conventional force balance were performed on a blunted cone of the same dimensions as used in HIEST.

Assuming the variation in each of the aerodynamic coefficients over angles of attack from 14° to 32° to be linear, the linear regression method was used for the uncertainty analysis of the present HIEST measurements. In the figures, the thick solid lines, dotted lines, and thin solid lines depict the least-squares fitting lines for HIEST condition 1, condition 2, and HWT2. The standard errors $\sigma_{\bar{x}}$ of all aerodynamic coefficients and degrees of freedom for each data-set (υ) are summarized in Table III. The precision of the measurements was defined as the 95%-PI (prediction interval), and is plotted as thin lines in the figures at the upper and lower uncertainty bounds. Since the 95%-PI of the HWT2 results was substantially smaller than those of HIEST, these uncertainty lines are not shown in the figures.

TABLE III. SE (standard error) of measurements under HIEST condition 1, condition 2 and HWT2.

	HIEST condition 1	HIEST condition 2	HWT2
υ	28	14	36
C_A	5.3×10^{-3}	5.9×10^{-2}	3.5×10^{-4}
C_N	8.1×10^{-3}	1.0×10^{-2}	4.9×10^{-4}
C_M	2.7×10^{-3}	4.6×10^{-3}	1.8×10^{-4}

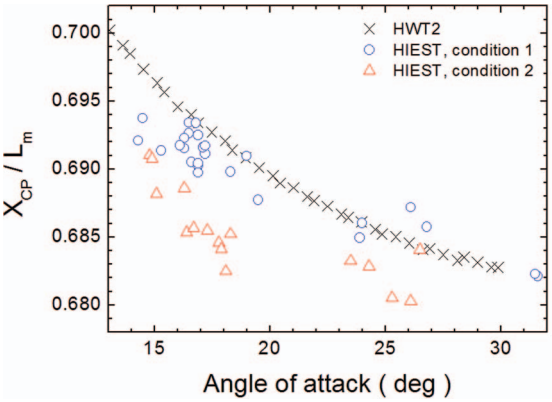

FIG. 13. Pressure-center versus angle of attack. Circles and triangles respectively show the results obtained under condition 1 and condition 2.

In order to estimate the present measurement accuracy, results under HIEST condition 1 and HWT2 were compared, as both cases can be considered as perfect-gas flows. As shown in Fig. 12, these two measurement groups agree to within their precisions, i.e., there is no significant difference in any of the aerodynamic coefficients (C_A, C_N, and C_M). This means we can be confident that the accuracy of the free-flight measurements in HIEST lies within the measurement uncertainties.

V. PITCHING MOMENT IN HIGH-TEMPERATURE REAL-GAS FLOW

As already mentioned in the Introduction, gas chemistry in high-temperature real-gas flows affects the pressure distribution around reentry vehicles, resulting in higher trim angles than in perfect-gas flows. Because of immature force-measurement technology, this trim-angle anomaly has not been detected previously in wind tunnel tests. The present measurement technique, however, would potentially allow us to see the difference in pitching-moment characteristics between perfect-gas and high-temperature real-gas flows. Thus, comparing now HIEST conditions 1 (perfect gas) and 2 (high-temperature real gas), we first note that the C_A and C_N coefficients agree to within their respective uncertainties (Figs. 12(a) and 12(b)), i.e., there is no significant difference observed in the two conditions. In contrast, C_M for condition 2 lies consistently above that of condition 1 (Fig. 12(c)); as the 95%-PI-bands do not overlap, this difference can be considered significant. These results demonstrate that the trim angle for condition 2 became larger (nose-up attitude) than for condition 1. Since the measurement discrepancy is not observed in C_A or C_N but only in C_M, it is thought to result from a c.p. shifting forward. Fig. 13 shows the determined c.p. versus angle of attack, which confirms the tendency of the c.p. to shift forward under condition 2. Both differences in Mach number and high-temperature real-gas effects might contribute to this shift. Considering that there is no significant difference between HIEST condition 1 (free-stream Mach number 7.6) and HWT2 (free-stream Mach number 9.7), however, it is most reasonable that high-temperature effects were the dominant cause of this c.p. shifting.

ACKNOWLEDGMENTS

The authors wish to thank to the HIEST technical staff Mr. Maehara, Mr. Narita, and Mr. Fujimura, who operate the HIEST facility.

[1]J. C. Young, L. F. Perez, P. O. Romere, and D. B. Kanipe, "Space Shuttle entry aerodynamic comparison of flight 1 with preflight predictions," AIAA Paper No. 81-2476, 1981.
[2]J. R. Maus, B. J. Griffith, K. Y. Szema, and J. T. Best, "Hypersonic Mach number and real gas effects on space Shuttle Orbiter Aerodynamics," J. Spacecr. Rockets **21**(2), 136–141 (1984).
[3]B. J. Griffith, J. R. Maus, B. M. Majors, and J. T. Best, "Addressing the hypersonic simulation problem," J. Spacecr. Rockets **24**(4), 334–341 (1987).
[4]K. Itoh, S. Ueda, H. Tanno, T. Komuro, and K. Sato, "Hypersonic aerothermodynamic and scramjet research using high enthalpy shock tunnel," Shock Waves **12**, 93–98 (2002).
[5]H. Tanno, T. Komuro, K. Sato, and K. Itoh, "Design and evaluation of strain gauge force balance with short test duration," Trans. Jpn. Soc. Aeronaut. Space Sci. **48**(159), 1–6 (2005).
[6]G. R. Duryea and W. J. Sheeran, "Accelerometer force balance techniques," ICIASF'69 record, 190–197 (1969).
[7]H. Tanno, "Experimental and numerical study to evaluate real-gas effects on generic models in the free-piston shock tunnel HIEST," in *Proceedings of the 6th European symposium on aerothermodynamics for space vehicles*, 2008.
[8]K. W. Naumann, H. Ende, and G. Mathieu, "Millisecond aerodynamic force measurement with side-jet model in the ISL," Shock Waves **1**, 223–232 (1991).
[9]L. Bernstein, *Force Measurement in Short-Duration Hypersonic facilities*, AGARD-AG-214, edited by R. C. Pankhurst (Technical Editing and Reproduction, London, 1975).
[10]H. Tanno, "Miniature data-recorder for aerodynamic force measurement in impulsive facility," AIAA Paper No. 2010-4204, 2010.
[11]S. J. Laurence and S. Karl, "An improved visualization-based force-measurement technique for short duration hypersonic facilities," Exp. Fluids **48**(6), 949 (2010).
[12]S. J. Laurence, "On tracking the motion of rigid bodies through edge detection and least-squares fitting," Exp. Fluids **52**(2), 387 (2012).
[13]M. Takahashi, "Influence of thermal non-equilibrium on nozzle flow condition of high enthalpy shock tunnel HIEST," AIAA Paper No. 2009-7267, 2009.
[14]M. Watari, N. Hirabayashi, T. Koyama, S. Nagai, S. Tsuda, H. Sekine, T. Yamazaki, and K. Nakakita, "Flow qualities of JAXA hypersonic wind tunnel facilities," AIAA Paper No. 2006-8047, 2006.